Published in final edited form as:
Phys Med Biol. 2008 August 21; 53(16): 4455–4470. doi:10.1088/0031-9155/53/16/016.

Assessment of the accuracy of an MCNPX-based Monte Carlo simulation model for predicting three-dimensional absorbed dose distributions

U Titt, **N Sahoo**, **X Ding**, **Y Zheng**, **W D Newhauser**, **X R Zhu**, **J C Polf**, **M T Gillin**, and **R Mohan**
The University of Texas M D Anderson Cancer Center, 1515 Holcombe Blvd., Houston, TX, 77030, USA

Abstract

In recent years, the Monte Carlo method has been used in a large number of research studies in radiation therapy. For applications such as treatment planning, it is essential to validate the dosimetric accuracy of the Monte Carlo simulations in heterogeneous media. The AAPM Report no 105 addresses issues concerning clinical implementation of Monte Carlo based treatment planning for photon and electron beams, however for proton-therapy planning, such guidance is not yet available. Here we present the results of our validation of the Monte Carlo model of the double scattering system used at our Proton Therapy Center in Houston. In this study, we compared Monte Carlo simulated depth doses and lateral profiles to measured data for a magnitude of beam parameters. We varied simulated proton energies and widths of the spread-out Bragg peaks, and compared them to measurements obtained during the commissioning phase of the Proton Therapy Center in Houston. Of 191 simulated data sets, 189 agreed with measured data sets to within 3% of the maximum dose difference and within 3 mm of the maximum range or penumbra size difference. The two simulated data sets that did not agree with the measured data sets were in the distal falloff of the measured dose distribution, where large dose gradients potentially produce large differences on the basis of minute changes in the beam steering. Hence, the Monte Carlo models of medium- and large-size double scattering proton-therapy nozzles were valid for proton beams in the 100 MeV–250 MeV interval.

Introduction

In 2006, The University of Texas, M D Anderson Cancer Center started treating patients at the newly built Proton Therapy Center in Houston (PTCH) (Smith *et al* 2003, Newhauser *et al* 2007b). The facility utilizes three identical passive scattering nozzles. Two are mounted on rotational gantries, and the other one is mounted in a fixed horizontal orientation. The dose distributions from these nozzles are of particular interest, because the nozzles are currently being used in clinical service. In the future, a scanned-beam nozzle and a low-energy ocular treatment nozzle will be commissioned. Pre-clinical preparation of the three passive scattering nozzles included the generation of measured and simulated proton field properties, including the lateral proton fluence, and absorbed-dose profiles and depth-dose profiles.

A validated Monte Carlo system for the simulation of radiation transport is a useful tool for pre-clinical and clinical research studies (Paganetti *et al* 2004). For example, Monte Carlo simulations have been used to provide dosimetric data for the configuration and testing of a commercial treatment planning system (Newhauser *et al* 2007b), assessment of dosimetric perturbations from implanted localization markers, stray radiation exposures to patients (Fontenot *et al* 2008), virtual commissioning of an ocular treatment planning system (Koch and Newhauser 2005), dose per monitor-unit predictions (Koch *et al* 2008), neutron shielding in a proton-therapy facility (Titt and Newhauser 2005), collimator scatter (Titt *et al* 2008) and in various other applications (Newhauser *et al* 2002a, 2002b, 2005a, 2005b, 2007a, 2007b, 2007c, Zhang *et al* 2007, Fontenot *et al* 2007, de Crevoisier *et al* 2007, Bues *et al* 2005, Zheng *et al* 2007a, Mourtada *et al* 2005, Fontenot *et al* 2005, Koch and Newhauser 2005, Polf *et al* 2005, 2007, Titt and Newhauser 2005, Polf and Newhauser 2005, Melancon *et al* 2007).

Despite its use in these applications, the dosimetric accuracy of M D Anderson's Monte Carlo proton-therapy simulation system has not been comprehensively validated, because the prerequisite beam data measurements are yet unavailable. In this work, we describe our efforts to validate the Monte Carlo simulation model of the double scattering nozzles used at the PTCH. We compared simulated beam data with experimental data measured during the clinical commissioning of the PTCH. Specifically, we compared simulations and measurements of lateral-dose profiles and per cent depth-dose profiles of proton beams with a range in water of 3.5 cm–28.5 cm. Dose distributions were obtained in a simple homogeneous water phantom and in a simple heterogeneous phantom that approximated a thorax. Standard figures of merit were used to quantitatively assess the levels of agreement between these data sets, including dose-difference and distance to agreement.

Materials and methods

Experimental set-up

Commissioning measurements in a homogeneous water phantom—The proton accelerator at the PTCH, a synchrotron, provides proton energies between 100 and 250 MeV. The beams are extracted from the accelerator and directed into the treatment rooms using magnetic fields that steer the beam through vacuum beam pipes. In the treatment rooms, the beam enters a nozzle housing beam-modifying devices, which change the beam parameters according to the requirements defined by the treatment plan. The passive scattering nozzles at the PTCH are composed of double scattering systems that include (1) a first scatterer that spreads the narrow proton beam upstream of a range modulator wheel (RMW), a rotating wheel with varying thicknesses that produces a spread-out Bragg peak (SOBP); and (2) a second scatterer that provides a uniform dose across the field size (Koehler *et al* 1977) at a specified depth (isocenter). At the PTCH, three different sets of beam-modifying devices are used to provide different field sizes: (1) the 'small snout', used for field sizes up to 10 cm × 10 cm; (2) the 'medium snout', used for field sizes up to 18 cm × 18 cm; and (3) the 'large snout', used for field sizes up to 25 cm × 25 cm. Each snout uses different first scatterers and second scatterers and a set of three RMWs, which provide the required uniformity of dose at the isocenter for any given range of the proton beam in water.

Because the energy of the proton beam entering the double scattering nozzle is divided into eight energy intervals, a set of range shifters, i.e., plastic slabs of varying thickness, is used to produce the required proton range with a resolution of 1 mm water-equivalent thickness. Detailed descriptions of the nozzle set-up have previously been published (Newhauser *et al* 2007b, Zheng *et al* 2007a).

Prior to clinical use, a set of commissioning measurements was performed for each RMW covering (among other parameters) the per cent depth doses (PDDs) and lateral-dose profiles in a water phantom for various proton ranges and SOBPs. The PTW MP3 water-tank scanning system and MEPHISTO mc^2 software (both from PTW, Freiburg, Germany) were used to measure the PDDs with an Advanced Markus parallel plate chamber (PTW model 340045, SN 293 or SN 0304) and cross-beam profiles with a PTW pinpoint chamber (PTW model 31006, SN 376 and SN 0079). A reference chamber was always used during data acquisition to control for dose-rate fluctuations of the beam. The water phantom was located with its upstream surface at a distance of 270 cm from the source (SSD = 270 cm), which is equal to the isocenter location. Some of the profiles were measured using EDR-2 films, which were scanned using a VIDAR Pro 16 scanner, and were analyzed using OmniPro-Accept 6.4 A software (Scanditronix Wellhöfer GmbH, Schwarzenbruck, Germany).

For all RMWs (except for the lowest proton energies), PDDs at full range and at minimum range (all range shifter plates in the beam) were recorded, and several SOBP widths were measured for each RMW. For each PDD, several lateral dose distributions were measured, typically at the center of the SOBP, 2 mm upstream of the distal edge (90% dose) and in the proximal region of the peak.

The snout holds a final collimator that conforms the beam to the lateral projection of the target. Square brass collimators with apertures of 23.4 cm × 23.4 cm and 16.6 cm × 16.6 cm (physical size, not projected to isocenter) were used in the large snout and in the medium snout, respectively. The reproducibility of the measured ranges (to the distal 90% depth) and SOBP widths (separation of distal 90% and proximal 95%) were within 1 mm. The chamber positioning uncertainties were estimated at less than 1 mm. The uncertainties in the measurement of flatness and symmetry of the profiles were estimated at less than 1%.

Proton beam scattering measurements in a heterogeneous phantom—Bone-equivalent plastic rods (density $\rho = 1.82$ g cm^{-3}, diameter = 2 cm, height = 20 cm) were located 2 mm downstream of the phantom wall, corresponding to a water-equivalent depth of 25 mm with a center-to-center distance of 3 cm. A 5 cm thick lung-equivalent plastic slab (density $\rho = 0.3$ g cm^{-3}) was then placed downstream of the rods. The elemental composition (vendor provided) of the bone-equivalent plastic was 2.41% H, 31.41% C, 1.84% N, 36.5% O, 0.04% Cl and 26.81% Ca. The lung-equivalent plastic was composed of 8.4% H, 59.38% C, 1.96% N, 18.14% O, 11.19% Mg, 0.78% Si and 0.1% Cl. PDDs and lateral-dose profiles were measured behind the slab for initial proton-beam energies of 225 MeV, 200 MeV and 180 MeV, which are typical proton energies used in thoracic treatments. The maximum ranges of these beams in water are 23.6 cm, 19.0 cm and 16.1 cm, respectively. The 180 MeV beam was measured once at full range and once with the minimum range (13.1 cm in water), i.e., with all range shifter plates in the beam line.

The depths of the lateral profiles were 20.8 cm and 16.2 cm for the 225 MeV and 200 MeV beams, respectively, and both 13.3 cm and 10.8 cm for the 180 MeV beam. (SSD = 270 cm) In all beams the SOBP width was 10 cm. All beams were delivered through an 8.3 cm × 8.3 cm aperture in the brass collimator, which was positioned 8 cm from the phantom surface for the 225 MeV and 200 MeV beams. This distance was 48 cm for the 180 MeV measurements. The variation in snout-to-water phantom distance was introduced to validate the Monte Carlo model with respect to changes in the lateral penumbra that occur due to the geometric changes in the set-up and due to potential changes in dose deposition from collimator scatter (Titt *et al* 2008).

Monte Carlo model

Homogeneous water phantom simulations—The Monte Carlo simulations in this study were carried out using the MCNPX code (version 2.5.0; LANL, Los Alamos, NM), a general-purpose radiation-transport-simulation code capable of simulating proton beams (Waters *et al* 2005). This code uses tabulated cross-sectional data up to a maximum energy, which is particle and material dependent, and beyond this maximum energy, the program uses model-based transport parameters. This code requires an input file that defines the geometry, physics parameters, and tallies of the simulated problem. The geometric set-up used in this study was developed by Newhauser *et al* (2007b) and Zheng *et al* (2007b).

The particle source and transport parameters were set as follows. The proton source was located at the upstream surface of the beam-exit window of the beam-delivery system. Its spatial distribution was described by two Gaussian distributions with a full-width half-maximum (FWHM) value of 0.54 cm in the *x*-direction and 1.22 cm in the *y*-direction. Additionally a so-called cookie-cutter cell was defined to limit the start position of the source particles to a radius of 3 cm around the beam axis. The energy of the protons was also modeled with Gaussian distributions, with a FWHM ranging from 0.23% for 250 MeV beams to 0.3% for 100 MeV beams of the nominal proton energy at the nozzle entrance. The energy spread was selected according to the specifications of the manufacturer of the synchrotron used at the PTCH. The initial direction of the source particles was parallel to the beam axis. The default kinetic energy cutoff value used was 1 MeV, at which the proton transport was terminated, and all remaining energy was deposited locally. The transport parameters were set to employ the ‘mix and match’ capability of the program, i.e., a smooth transition was realized when the transport was changing from model-based parameters to tabulated parameters. Straggling was performed with the Vavilov model (Vavilov 1957), and light-ion recoil was suppressed.

The geometries were detailed models of the medium- and large-size nozzles, comprising the beam-modifying devices, which are present in the physical nozzles. The parts were modeled according to material specifications and structural designs provided by the vendor (Hitachi Ltd, Japan). A schematic of the design is shown in figure 1. Detailed descriptions have been provided by Newhauser *et al* (2007b) and Zheng *et al* (2007b).

A mesh tally was located in the water phantom, which provided energy deposition per unit volume per particle history in units of MeV cm^{-3} n^{-1}. In water (density $\rho = 1$ g cm^{-3}), this value corresponds to the dose deposited per particle history in units of MeV g^{-1} n^{-1}. The

spatial resolution of the tally was 1 mm × 8 cm × 1 mm for simulations of the large snout and 1 mm × 4 cm × 1 mm for simulations of the medium snout. The large size of the tally in one direction was implemented to decrease statistical uncertainty in the results, and the orientation was set perpendicular to the beam axis and to the plane of interest (i.e., in the case of a lateral profile in the *x*-direction, the large side of the tally would be in the *y*-direction and vice versa). The only variance reduction technique applied in the simulations was weighted-particle splitting of particles entering the water phantom.

The modulation widths of the SOBPs are determined by the gate-off angles of the rotating RMW at which the beam would be turned on and off, so that the beam penetrates the correct thickness of material on the RMW. To generate an SOBP from the simulated data, single Bragg peaks were simulated separately and subsequently combined with post-processing software. The RMW rotation angle was quantized in 3° increments. Each peak was simulated with 10^7 source particles to achieve statistical uncertainties of less than 1% in the region of interest.

Proton beam scattering simulations in the heterogeneous phantom—The model of the inhomogeneity set-up comprised the same snout set-up and water phantom from the commissioning simulations with the addition of bone-equivalent plastic rods (density ρ = 1.82 g cm^{-3}) that were inserted in the water phantom at the water-equivalent depths of 25 mm, corresponding to the water-equivalent thickness of the position of the rods in the measurements, followed by a 5 cm lung-equivalent slab with a density of 0.3 g cm^{-3}. The transport physics, the tally type, and the dimensions were similar to those of the commissioning simulations. The compositions of the bone-equivalent and lung-equivalent materials are given in table 1.

Comparing simulated and measured dose profiles

Homogeneous water phantom data—The goal of this study was to compare measured dose profiles to Monte Carlo simulated dose profiles for all RMWs. PDDs were normalized to the dose at the center of the SOBP, and lateral profiles were normalized to the average value in the high-dose region, corresponding to 80% of the field size. Three distinct lateral penumbra widths were investigated: the spatial difference between the 90% and 10% dose locations, the 90% and 50% dose locations and the 80% and 20% dose locations. The proton ranges were determined at the 90% dose location at the distal edge of the beam. The SOBP width was determined between the distal 90% and the proximal 95% of the peak region (see figure 2).

The validation criteria were as follows: maximum difference in dose ≤3% (in a high-dose region), maximum difference in range or penumbra width ≤3 mm, and maximum difference in SOBP width ≤10 mm. The rather large tolerance for the SOBP width is based on the fact that the proximal 95% dose location is typically positioned in a low-dose-gradient region, where a small change in the dose leads to large changes in the SOBP width. A total of 63 simulated PDDs and 126 simulated lateral-dose profiles were compared with the corresponding measured parameters.

Proton beam scattering data in a heterogeneous phantom—All lateral profiles were normalized to the central axis values. The PDDs were normalized to the values at the center of the SOBPs. The data were then compared in terms of difference in dose, range and penumbra size with acceptance criteria similar to those in the commissioning data.

Results

Homogeneous water phantom data

Figure 2 compares the PDDs obtained from Monte Carlo simulated and measured doses. The PDDs of a beam with maximum range of 28.5 cm (250 MeV at nozzle entrance) in the medium snout is shown for two different SOBP widths (10 cm and 4 cm) measured from the distal 90% to the proximal 95% dose locations. Also shown is the PDD of a beam with an energy of 120 MeV at the nozzle entrance for a SOBP width of 1 cm.

Figure 3 shows a comparison of simulated and measured lateral profiles. The penumbra widths (dotted lines) were measured from the 90% to the 50% dose locations, from the 90% to the 10% dose locations and from the 80% to the 20% dose locations. The field size was determined from the distance between the 50% dose locations. The figure also shows the statistical uncertainties (1 σ confidence interval) associated with the simulated data.

The results of the comparison of simulated and measured PDDs using the large snout are given in table 2 for different proton energies (E_p) at the nozzle entrance and the various ranges. The parameters used for comparison are range at the distal 90% dose location (r_{90}); SOBP width (m); and maximum absolute dose difference (ΔD_{max}), which is given as a percentage of the normalization value at the center of the SOBP. The differences between measured and simulated values for 90% dose location and SOBP width are tabulated as Δr_{90} and Δm, respectively. In some cases, measured data were unavailable, so the differences were determined between the simulated data and the nominal values of r_{90} or m, respectively.

The results of the comparison of simulated and measured lateral profiles for the large snout are shown in table 3 for different proton energies, E_p; SOBP widths, m; and depths (z) of the profile relative to the upstream surface of the water phantom, which was located at the isocenter. The absolute differences in the penumbra widths are denoted as $\Delta P_{90–10}$ for the values of the 90%–10% penumbras, $\Delta P_{90–50}$ for the values of the 90%–50% penumbras and $\Delta P_{80–20}$ for the absolute differences in the 80%–20% penumbras. The absolute difference in field size is denoted by ΔFS. The maximum dose difference, ΔD_{max}, in the high-dose region of the profile is given as a percentage of the dose, normalized to the center region of the profile. Similar data for the medium snout are available directly from the authors.

Comparison of the PDD data showed that the median difference between measured and simulated PDD was about 1 mm, and the maximum difference was 2.3 mm. All simulated values were considered acceptable because they agreed with measurement values to within the validation criteria of 3 mm. Figure 4(a) shows the frequency distribution, f, of the absolute range differences. There was no apparent correlation between the range differences and any of the beam parameters. The frequency distribution of the SOBP widths is shown in

figure 4(b), which shows a distribution with a maximum of about 7 mm, where 3 of 63 values are larger than 5 mm. The frequency distribution of the maximum dose difference found in PDDs is shown in figure 4(c), which shows a mean value of about 2% of the dose at the center of the SOBP. Eight of 63 simulated PDDs showed a dose difference of 3% compared to the measured curves. Higher dose differences were found at small proton energies, especially at small SOBP widths. However all dose differences were considered acceptable. The absolute values of the maximum dose differences in the lateral profiles are shown in figure 4(d). The distribution also shows extreme outliers, one at 3.6% and another at 4%. These values would be unacceptable. A closer look at the data revealed that both values were derived when simulation data were compared to asymmetric measured curves obtained in the distal falloff of the fields. One possible explanation for the asymmetry is that small changes in beam steering can introduce large asymmetries in the measurements in the high-dose-gradient falloff region. Another possible explanation is that a positioning error of the experimental set-up biased the effective point of the measurement. If the normal vector of the phantom's surface has a slight angle with respect to the beam axis, an asymmetry would result. Whatever may be the reason for the measured asymmetry, the simulation of the profiles cannot account for 'real world' imperfections, and hence are not considered a failure.

Figure 5(a) shows the frequency distribution of the absolute differences in the 90%–10% penumbra of the lateral profiles. The mean value is 0.8 mm, and the maximum difference was 2.3 mm. Only 2 of 126 values are between 2 and 2.5 mm. Figure 5(b) shows the distribution of the differences in the 90%–50% penumbral width between the simulated and the measured data. All $\Delta P_{90–50}$ penumbral widths were smaller than 1.2 mm, and the mean value is about 0.4 mm. Figure 5(c) shows the data of the 80%–20% differences (absolute values). Only 1 of $\Delta P_{80–20}$ 126 values is larger than 1.5 mm. The mean value of the distribution is about 0.5 mm. Figure 5(d) shows the absolute values of the field-size difference distribution in millimeters. The mean difference in field size between simulations and measurements was about 0.4 mm. Only 2 of 126 values were larger than 1 mm.

Proton scattering results in the heterogeneous phantom

Table 4 summarizes the results of the comparison of simulations and measurements in the heterogeneous phantom containing bone- and lung-equivalent plastic devices (see also figures 6 and 7). The maximum dose difference of about 2% of the dose at the center of the SOBP was found in the PDD with the largest range, all other dose differences were smaller than 2%. The differences in the 80%–20% penumbras as well as the differences in ranges, were found to be smaller than or equal to 1.5 mm.

Discussion

In this study, we confirmed the dosimetric accuracy of the Monte Carlo model used at our PTCH by comparing its simulations of PDDs and lateral-dose profiles with measurements from a passive scattering proton treatment unit. The comparison included all range modulators, all scattering devices and two phantoms. The overwhelmingly good agreement

between measured and simulated data suggests that the model is sufficiently accurate for use in clinical applications, such as treatment planning calculations.

This study offers several benefits. First, it is among the most comprehensive efforts ever made to validate the use of the Monte Carlo method for proton-therapy dose calculations. In addition, it examined a contemporary, commercially available treatment system that is of considerable clinical relevance. As well, this study was the logical extension of earlier works in this area, which have validated the MCNPX-based simulations for specific proton energies only, such as the study of the 250 and 180 MeV (medium-size) snouts ((Polf *et al* 2007); the study of an ocular treatment nozzle for very small fields and proton energies, i.e., below 100 MeV (Newhauser *et al* 2005a), the study of absorbed dose per monitor unit in an ocular treatment nozzle (Koch *et al* 2008), and the study of the dosimetric impact of tantalum markers in ocular treatments (Newhauser *et al* 2007c). The scope of our results, however, is much more comprehensive due the inclusion of all possible energies for the medium- and large-size double scattering snouts.

Another benefit of this study is that it validated dose predictions in a simple water phantom and in a heterogeneous phantom. In addition, our MCNPX model was robust, requiring only a detailed model of the beam-line geometry and selection of appropriate physics model parameters; no empirical adjustments to the model or corrections to the data were necessary.

One limitation of this study is the approximate treatment of the proton phase space as each proton history began. In particular, we approximated the starting proton beam as having zero emittance, whereas the manufacturer's analytical calculations of the beam optics indicated the emittance was small but not zero. This does not appear to be a serious limitation, because the radiation-field properties in the phantoms were predominated by scattering in the nozzle components and in the phantom rather than by the emittance of the initial beam. In magnetically scanned nozzles, there is much less material in the beam path; therefore, the initial emittance of the beam may be more important in that setting. Another limitation is that we did not look as small field sizes. The reason was that experimental data were not available for such an analysis; however, this work is now in progress

The validation of the Monte Carlo system facilitates further development of advanced methods, algorithms and technologies. It confirms that the physics models are of sufficient accuracy for calculating relative dose distributions. Additional validation is still needed for small field sizes and for absolute dosimetry in terms of dose per monitor unit. However, future validation efforts will probably need to focus more on computer programming errors and less on the suitability of the physics models contained with the MCNPX code.

It is noteworthy that many of the simulation results were not optimized, i.e., the parameters of the model were not further refined once the results were within the acceptance criteria. This, in turn, means that the results presented in this study represent a scenario that is not necessarily the best case. Although all beams for the medium and large snouts can be simulated within tolerance limits, there is still the potential to improve simulation results. The results obtained by Polf *et al* (2007) indicate that substantial changes in the proximal region of a PDD can be achieved by changing the spatial size parameters of the proton

source. The proximal region of the PDDs showed the largest discrepancies between simulated and measured data in this study (see figure 2). The discrepancies shown here may be caused by a shortcoming of accurately modeling the source. Possible other causes include small errors in the physics models used in the particle transport, small errors in the nuclear reaction cross sections, or the suppression of transport of secondary particles other than protons.

Also the efficiency of the Monte Carlo model has yet to be optimized, and there are many possible improvements to be implemented, such as additional variance reduction methods and an optimized choice of particle transport parameters, such as the energy cutoff value at which the proton transport will be terminated. The default value of 1 MeV was used in this study, but the range of a proton with the energy of 1 MeV in water is only about 27 μm, and a 1 mm range corresponds to a proton energy of about 9 MeV. Carefully chosen transport parameters can significantly improve the computation speed of the Monte Carlo system

Future studies underway at our institution will validate the Monte Carlo model to simulate the small double scattering snout of the PTCH, which provides field sizes up to 10 cm×10 cm, the actively scanned proton beam line and the ocular beam line.

Conclusion

The MCNPX-based Monte Carlo model of the nozzle for a passively scattered proton beam at the PTCH used to simulate dose distributions was found to be accurate after extensive comparison with measured dose distributions in a simple homogeneous water phantom and in a heterogeneous phantom. The results of this study will allow us to use this model in our study of dose distribution in more complex geometries, inhomogeneous media and patients. In 2 of 191 data sets, the maximum dose differences between measured and simulated dose profiles were larger than the tolerance criterion of maximum 3% dose difference and 3 mm distance to agreement; however, it was determined that these cases were lateral profiles in the distal falloff region, where the measured data showed large asymmetries probably due to small fluctuations in the beam steering. These two cases were plausibly explained and hence considered acceptable. Because the Monte Carlo system performed well over a wide range of proton energies, SOBP width and even in a heterogeneous phantom, containing heterogeneities of bone- and lung-equivalent material, it can be concluded that the physics implemented in MCNPX is adequate, and hence the code provides an excellent tool for applications in the radiotherapy environment, in particular, in proton therapy.

Furthermore, the AAPM Report no 105 addresses issues concerning clinical implementation of Monte Carlo based treatment planning systems for photon and electron radiation treatments. Validation of the Monte Carlo model is considered an integral part of the commissioning process of a treatment planning system. For proton therapy, no such document has been published yet. This study will therefore be of great interest for the charged particle treatment planning community.

Acknowledgments

The authors wish to express their gratitude to the Monte Carlo research team of the Department of Radiation Physics at The University of Texas M D Anderson Cancer Center for developing the beam line model and for supporting these validation efforts. Furthermore, we would like to thank the clinical physics team at the PTCH for providing the experimental data collected during the commissioning of the double scattering nozzles.

References

Bues M, Newhauser WD, Titt U, Smith AR. Therapeutic step and shoot proton beam spot-scanning with a multi-leaf collimator: a Monte Carlo study. Radiat. Prot. Dosim. 2005; 115:164–169.

de Crevoisier R, et al. Changes in the pelvic anatomy after an IMRT treatment fraction of prostate cancer. Int. J. Radiat. Oncol. Biol. Phys. 2007; 68:1529–1536. [PubMed: 17544595]

Fontenot J, Taddei P, Zheng Y, Mirkovic D, Jordan T, Newhauser WD. Equivalent dose and effective dose from stray radiation during passively scattered proton radiotherapy of the prostate. Phys. Med. Biol. 2008; 53:1677–1688. [PubMed: 18367796]

Fontenot JD, Newhauser WD, Bloch C, White RA, Titt U, Starkschall G. Determination of output factors for small proton therapy fields. Med. Phys. 2007; 34:489–498. [PubMed: 17388166]

Fontenot JD, Newhauser WD, Titt U. Design tools for proton therapy nozzles based on the double-scattering foil technique. Radiat. Prot. Dosim. 2005; 116:211–215.

Koch N, Newhauser W. Virtual commissioning of a treatment planning system for proton therapy of ocular cancers. Radiat. Prot. Dosim. 2005; 115:159–163.

Koch N, Newhauser WD, Titt U, Gombos D, Coombes K, Starkschall G. Monte Carlo calculations and measurements of absorbed dose per monitor unit for the treatment of uveal melanoma with proton therapy. Phys. Med. Biol. 2008; 53:1581–1594. [PubMed: 18367789]

Koehler AM, Schneider RJ, Sisterson JM. Flattening of proton dose distributions for large-field radiotherapy. Med. Phys. 1977; 4:297–301. [PubMed: 407436]

Melancon AD, et al. Is a 3-mm intrafractional margin sufficient for daily image-guided intensity-modulated radiation therapy of prostate cancer? Radiother. Oncol. 2007; 85:251–259. [PubMed: 17892900]

Mourtada F, Koch N, Newhauser W. 106Ru/106Rh plaque and proton radiotherapy for ocular melanoma: a comparative dosimetric study. Radiat. Prot. Dosim. 2005; 116:454–460.

Newhauser W, Fontenot J, Koch N, Dong L, Lee A, Zheng Y, Waters L, Mohan R. Monte Carlo simulations of the dosimetric impact of radiopaque fiducial markers for proton radiotherapy of the prostate. Phys. Med. Biol. 2007a; 52:2937–2952. [PubMed: 17505081]

Newhauser W, Fontenot J, Zheng Y, Polf J, Titt U, Koch N, Zhang X, Mohan R. Monte Carlo simulations for configuring and testing an analytical proton dose-calculation algorithm. Phys. Med. Biol. 2007b; 52:4569–4584. [PubMed: 17634651]

Newhauser W, Koch N, Hummel S, Ziegler M, Titt U. Monte Carlo simulations of a nozzle for the treatment of ocular tumours with high-energy proton beams. Phys. Med. Biol. 2005a; 50:5229–5249. [PubMed: 16264250]

Newhauser WD, Burns J, Smith AR. Dosimetry for ocular proton beam therapy at the Harvard Cyclotron Laboratory based on the ICRU Report 59. Med. Phys. 2002a; 29:1953–1961. [PubMed: 12349914]

Newhauser WD, Ding X, Giragosian D, Nill S, Titt U. Neutron radiation area monitoring system for proton therapy facilities. Radiat. Prot. Dosim. 2005b; 115:149–153.

Newhauser WD, Koch NC, Fontenot JD, Rosenthal SJ, D SG, Fitzek MM, Mohan R. Dosimetric impact of tantalum markers used in the treatment of uveal melanoma with proton beam therapy. Phys. Med. Biol. 2007c; 52:3979–3990. [PubMed: 17664589]

Newhauser WD, Myers KD, Rosenthal SJ, Smith AR. Proton beam dosimetry for radiosurgery: implementation of the ICRU Report 59 at the Harvard Cyclotron Laboratory. Phys. Med. Biol. 2002b; 47:1369–1389. [PubMed: 12030561]

Paganetti H, Jiang H, Lee SY, Kooy HM. Accurate Monte Carlo simulations for nozzle design, commissioning and quality assurance for a proton radiation therapy facility. Med. Phys. 2004; 31:2107–2118. [PubMed: 15305464]

Polf JC, Harvey MC, Titt U, Newhauser WD, Smith AR. Initial beam size study for passive scatter proton therapy: I. Monte Carlo verification. Med. Phys. 2007; 34:4213–4218. [PubMed: 18072485]

Polf JC, Newhauser WD. Calculations of neutron dose equivalent exposures from range-modulated proton therapy beams. Phys. Med. Biol. 2005; 50:3859–3873. [PubMed: 16077232]

Polf JC, Newhauser WD, Titt U. Patient neutron dose equivalent exposures outside of the proton therapy treatment field. Radiat. Prot. Dosim. 2005; 115:154–158.

Smith, AR.; Newhauser, WD.; Latinkic, M.; Hay, A.; McMaken, B.; Styles, J.; Cox, J. The University of Texas M D Anderson Cancer Center proton therapy facility; Proc. 17th Int. Conf. Application of Accelerators in Research and Industry; 2003. p. 1073-1076.

Titt U, Newhauser WD. Neutron shielding calculations in a proton therapy facility based on Monte Carlo simulations and analytical models: criterion for selecting the method of choice. Radiat. Prot. Dosim. 2005; 115:144–148.

Titt U, Zheng Y, Vassiliev ON, Newhauser WD. Monte Carlo investigation of collimator scatter of proton-therapy beams produced using the passive scattering method. Phys. Med. Biol. 2008; 53:487–504. [PubMed: 18185001]

Vavilov PV. Ionization losses of high-energy heavy particles. Sov. Phys.—JETP. 1957; 5:749.

Waters, LS.; Hendricks, J.; McKinney, G. MCNPX version 2.5.0. Los Alamos: Los Alamos National Laboratory; 2005.

Zhang X, Dong L, Lee AK, Cox JD, Kuban DA, Zhu RX, Wang X, Li Y, Newhauser WD, Gillin M, Mohan R. Effect of anatomic motion on proton therapy dose distributions in prostate cancer treatment. Int. J. Radiat. Oncol. Biol. Phys. 2007; 67:620–629. [PubMed: 17236979]

Zheng Y, Newhauser W, Fontenot J, Taddei P, Mohan R. Monte Carlo study of neutron dose equivalent during passive scattering proton therapy. Phys. Med. Biol. 2007a; 52:4481–4496. [PubMed: 17634645]

Zheng Y, Newhauser WD, Fontenot J, Koch N, Mohan R. Monte Carlo simulations of stray neutron radiation exposures in proton therapy. J. Nucl. Mater. 2007b; 361:289–297.

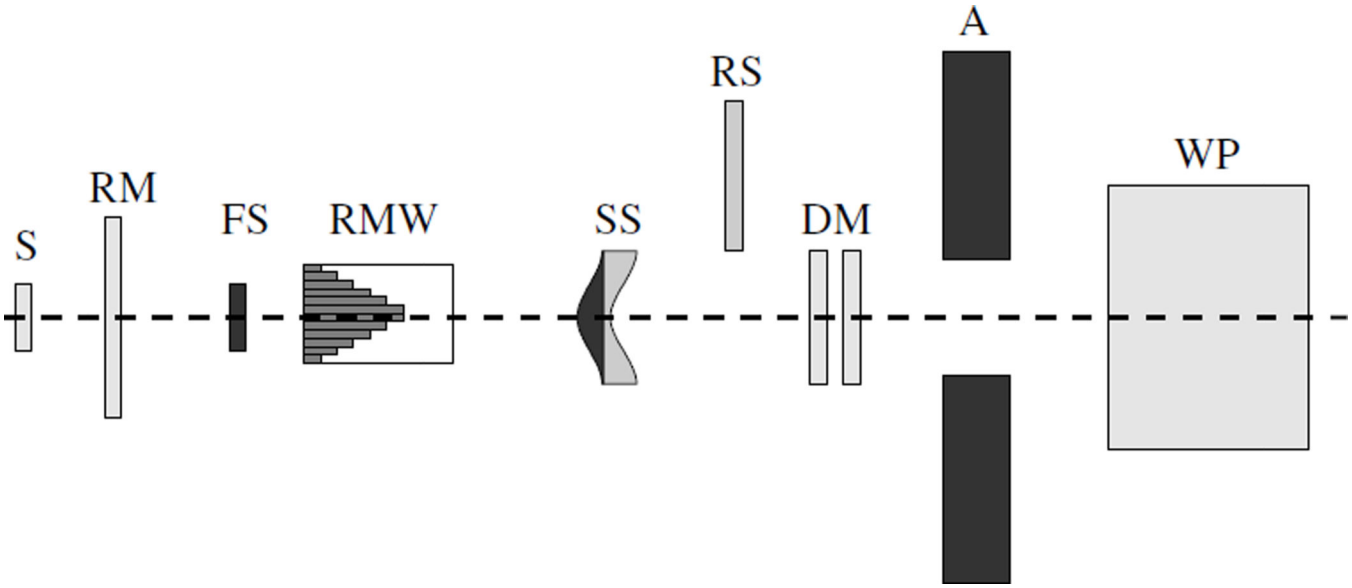

Figure 1.

Schematic drawing of the Monte Carlo model of the nozzle. The proton source (S) is located on the left. Downstream of a reference monitor (RM) chamber, the first scatterer (FS) is located upstream of the range modulator wheel (RMW). A second scatterer (SS) follows, and downstream of the SS, range shifters (RS) are positioned so that they can be inserted into the beam if the range has to be adjusted. Following these scatterers, two dose monitors (DM) are located upstream of a brass collimator (A). Finally, the beam enters the water phantom (WP) on the right.

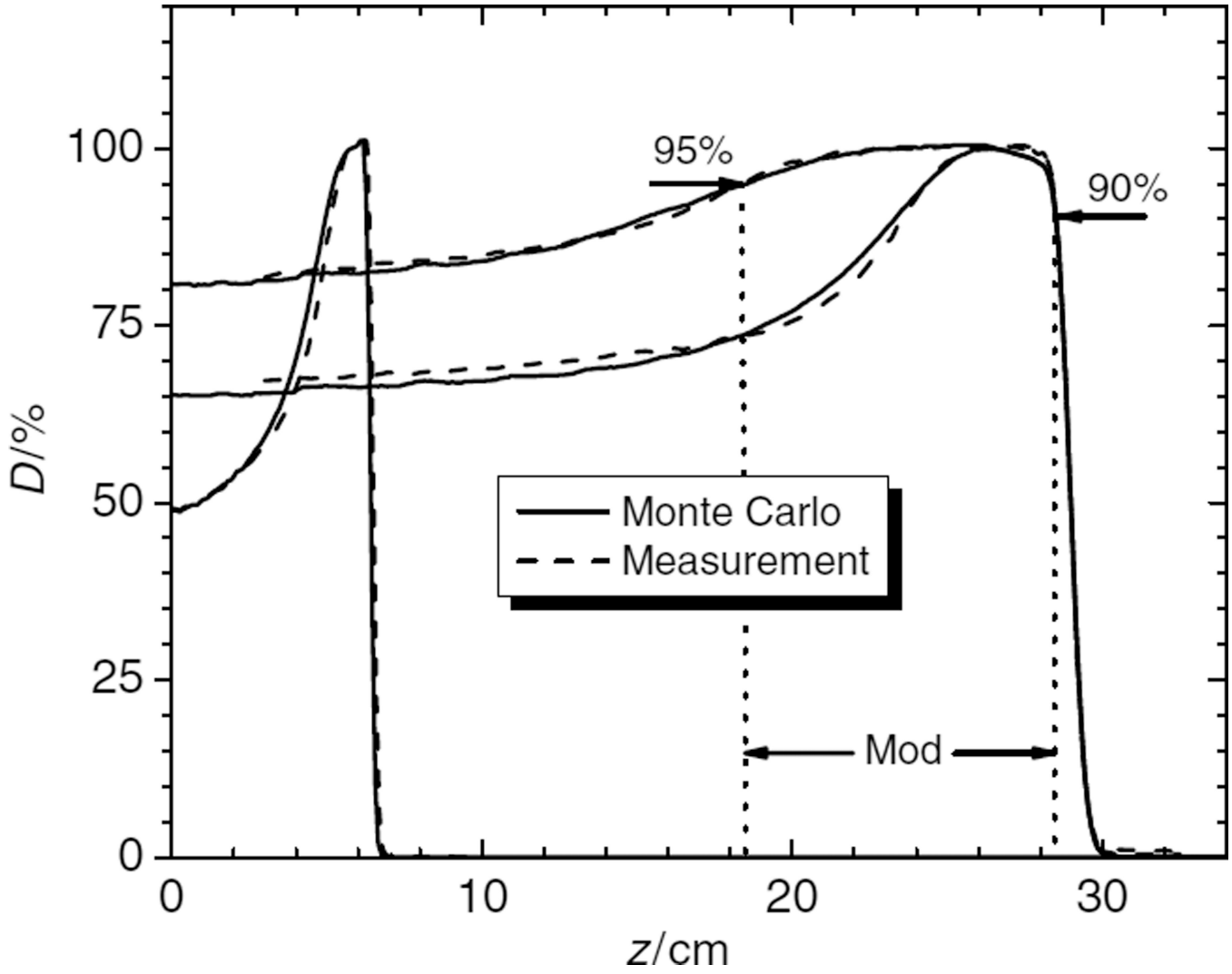

Figure 2.

Typical comparison of PDDs. The high-energy beam (250 MeV) is shown with two different SOBP widths (4 cm and 10 cm), and a low-energy beam (120 MeV) is shown with a 1 cm SOBP width. The SOBP (mod) width is defined from the distal 90% to the 95% proximal dose location. There are differences in the proximal region of the peaks, but these are still within tolerance limits.

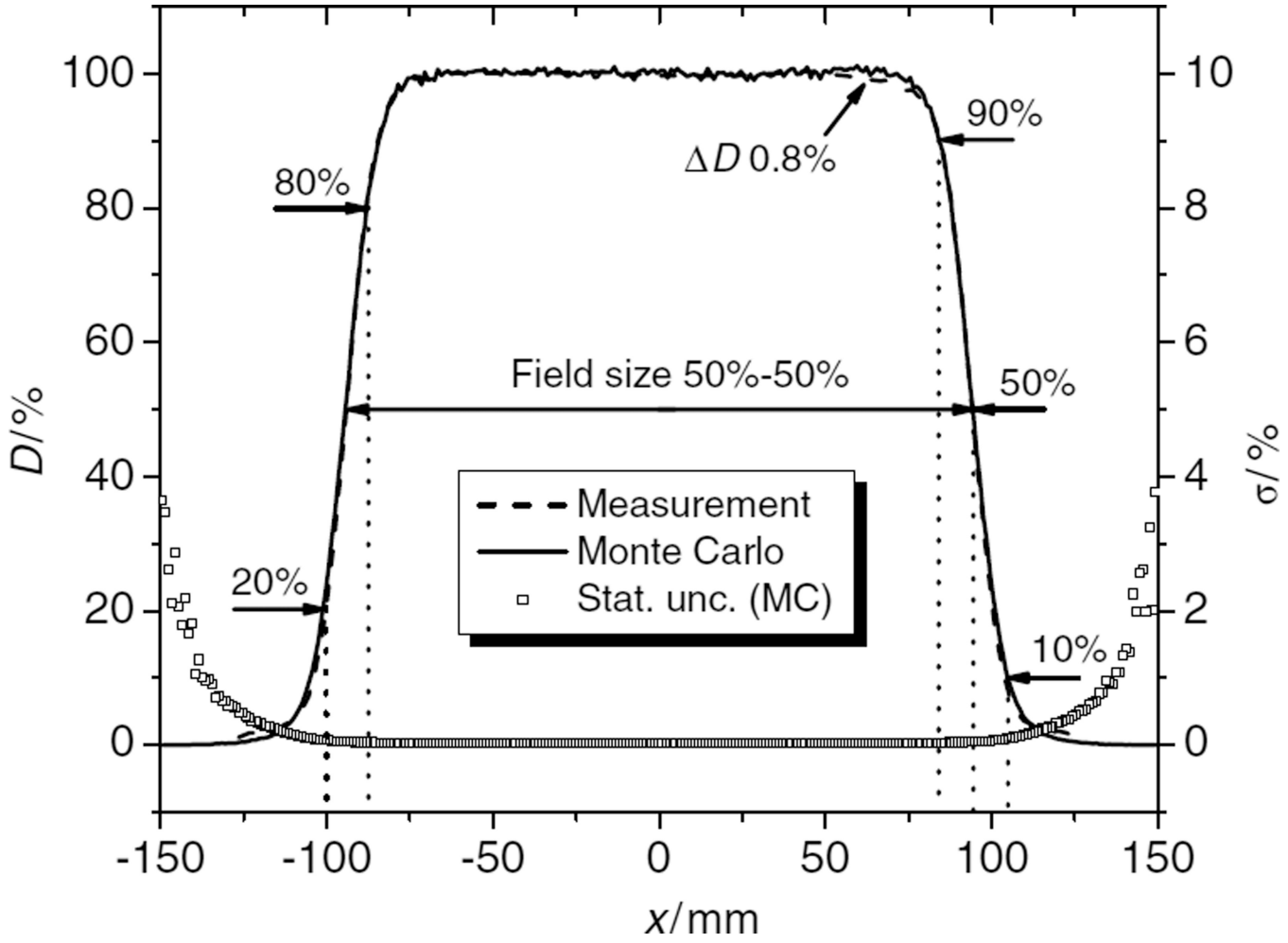

Figure 3.

Example of comparison of lateral dose profiles (left-side scale). These profiles were obtained at a depth of 28.3 cm. The beam had full range (28.5 cm in water, 250 MeV at nozzle entrance) and had a SOBP width of 16 cm. The dotted lines show where the penumbras were measured and the field size was determined from the distance between the 50% dose points. At the right edge of the field, a dose difference (ΔD) of 0.8% is shown. Additionally, the relative statistical uncertainty, σ, of the simulation data is shown in this graph (right-side scale).

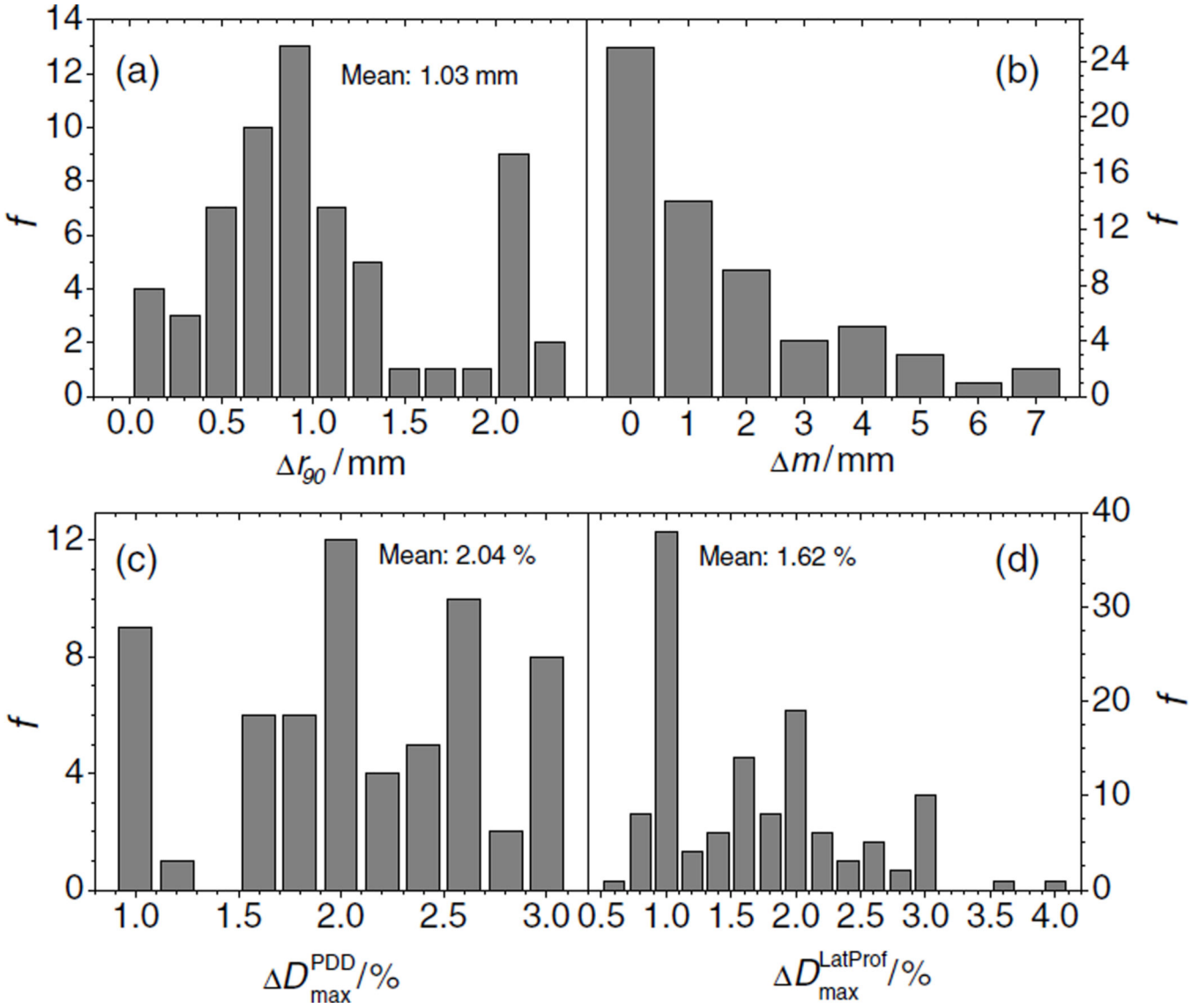

Figure 4.

(a) Frequency distribution, *f*, of the absolute differences of ranges between measured and simulated SOBPs. The mean value is 1.03 mm. (b) Frequency distribution, *f*, of the absolute differences in SOBP width, *m*, between measured and simulated PDDs. (c) Frequency distribution of the maximum absolute differences in dose between measured and simulated PDDs. (d) Frequency distribution. *f*, of the absolute differences in dose between measured and simulated lateral profiles.

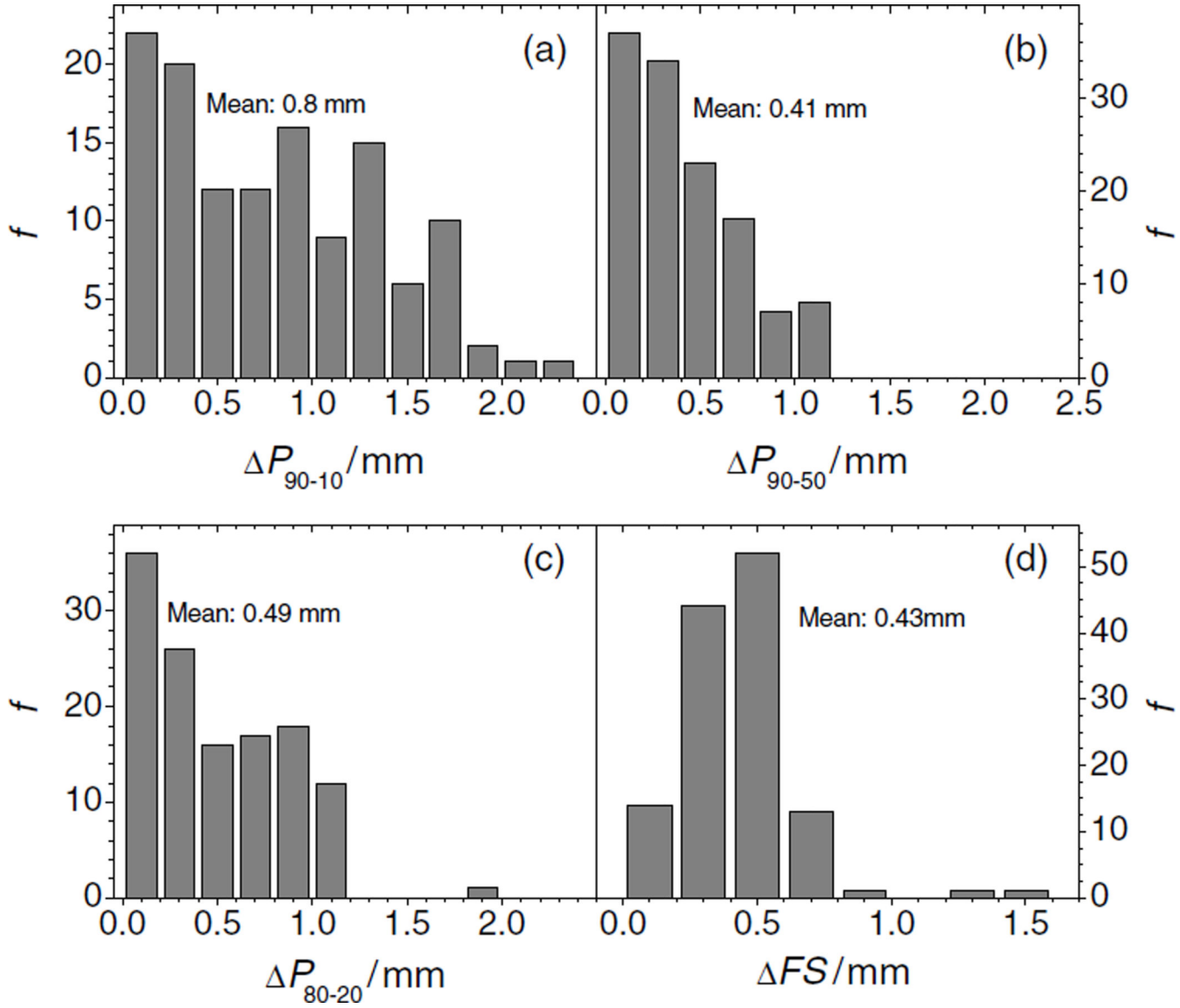

Figure 5.

Frequency distribution, *f*, of the absolute differences of penumbras between measured and simulated lateral profiles. The differences in the 90%–10% penumbra (ΔP_{90-10}) are shown in panel (a), the values for the 90%–50% penumbra (ΔP_{90-50}) are shown in panel (b), and the absolute differences in the 80%–20% penumbra are shown in panel (c). Panel (d) depicts the frequency distribution, *f*, of the absolute differences in field size (ΔFS).

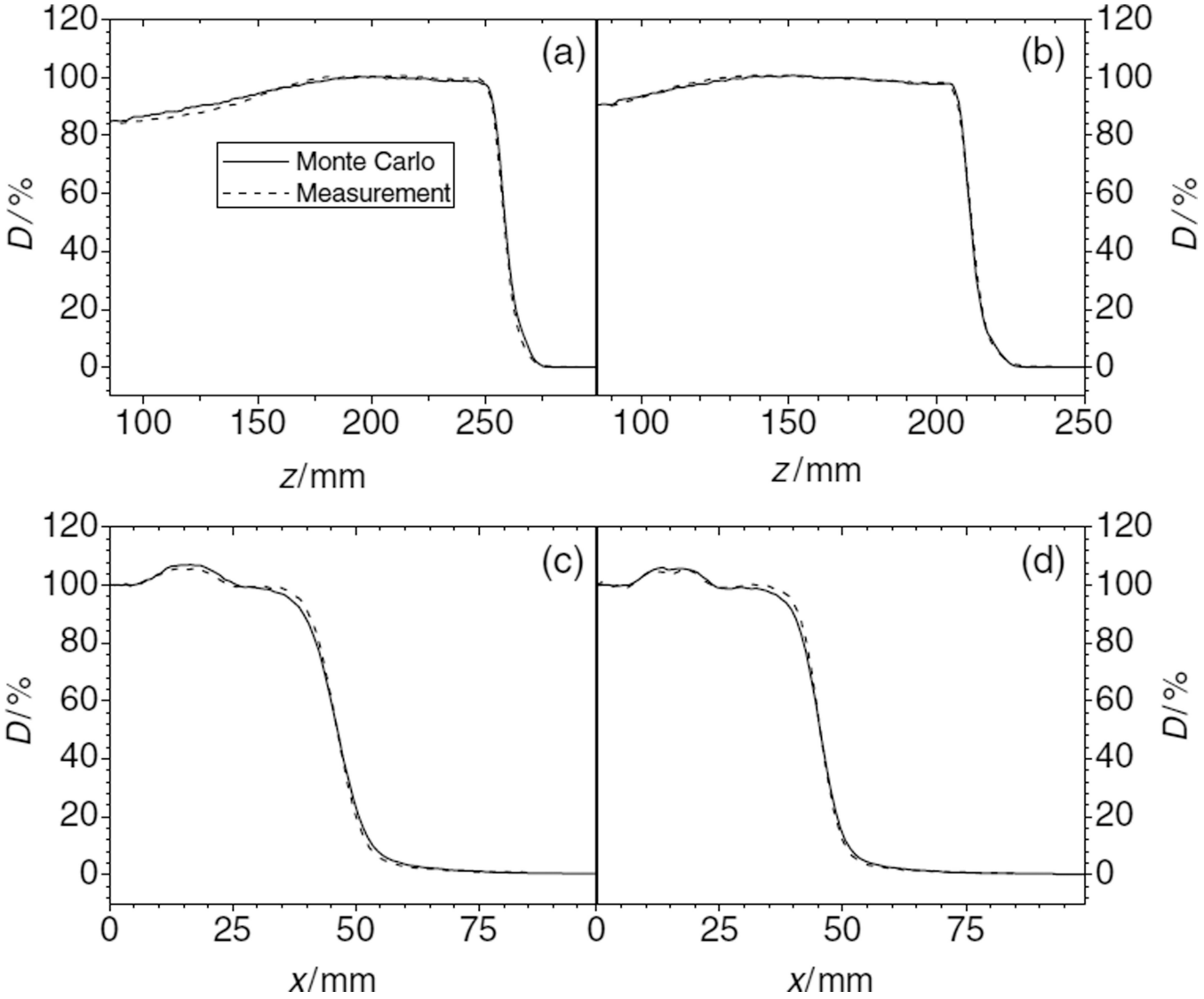

Figure 6.

PDDs (panels (a) and (b)) and lateral profiles (panels (c) and (d)) of proton dose downstream of the inhomogeneity set-up. Initial proton beam energy was 250 MeV (panels (a) and (c)) and 200 MeV (panels (b) and (d)). The depths, *z*, of the lateral profiles in the phantom were 20.8 cm (c) and 16.2 cm (d).

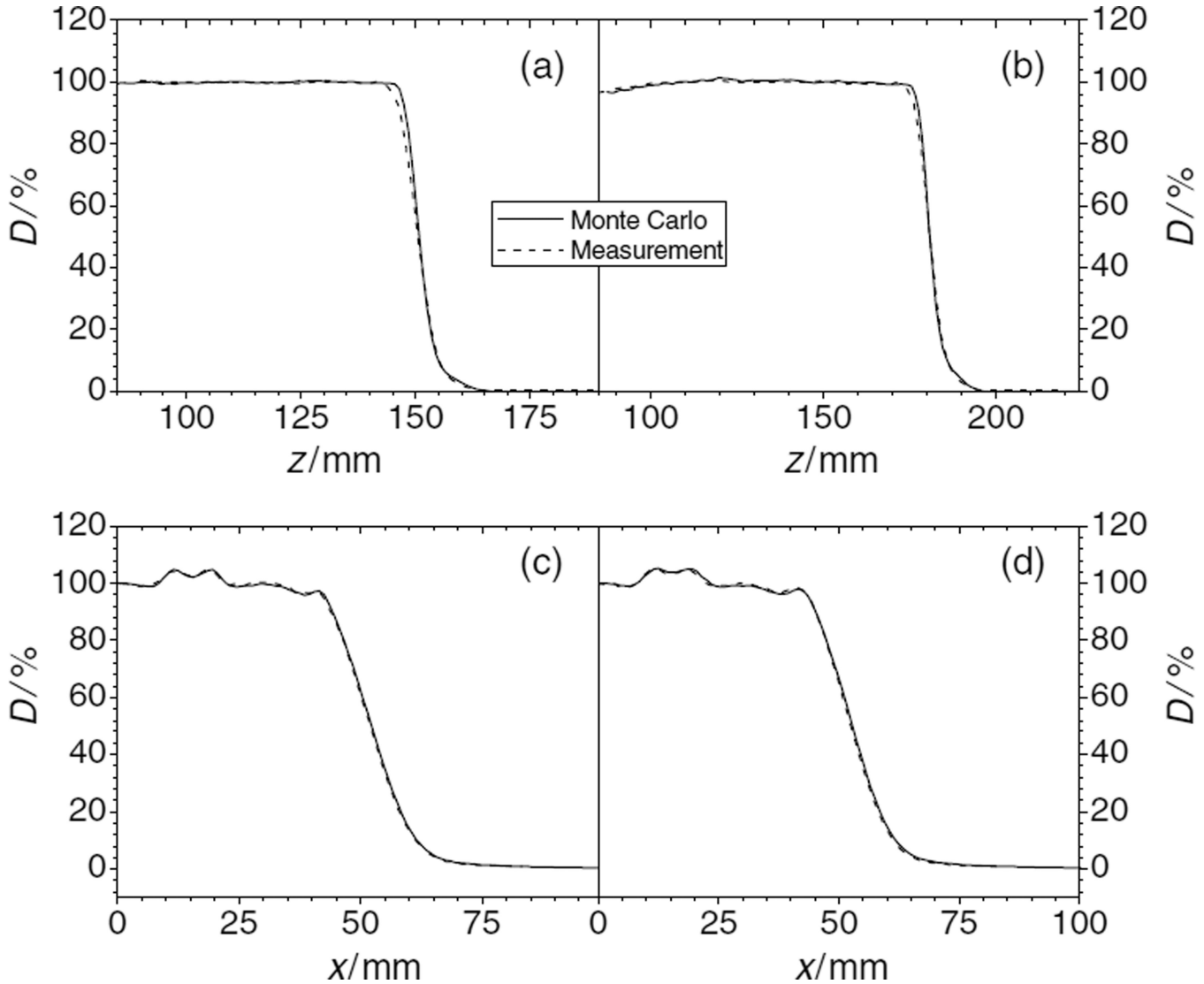

Figure 7.

PDDs and lateral profiles of proton dose downstream of the inhomogeneity set-up. The initial proton beam energy was 180 MeV. Panels, (a) and (c), show the data obtained with range shifters in the beam line. The depths, *z*, of the lateral profiles in the phantom were 10.8 cm (c) and 13.3 cm (d).

Table 1

Atomic composition of the lung-equivalent and bone-equivalent materials used in the Monte Carlo simulations.

Lung		Bone	
Element	**Atomic fraction**	**Element**	**Atomic fraction**
H	0.64	H	0.47
C	5.45×10^{-2}	C	0.12
N	1.38×10^{-2}	N	3.04×10^{-2}
O	0.29	O	0.28
Na	5.43×10^{-4}	Mg	9.18×10^{-4}
P	4.03×10^{-4}	P	3.44×10^{-2}
S	5.843×10^{-4}	S	9.97×10^{-4}
Cl	5.28×10^{-4}	Ca	5.31×10^{-2}
K	3.19×10^{-4}	Zn	1.55×10^{-5}

Table 2

Comparison of simulated PDDs to measured PDDs in the large snout. E_p is the proton energy at nozzle entrance, r_{90} is the nominal range at the distal 90% dose location, and m is the nominal SOBP width of the SOBP.

E_p (MeV)	r_{90} (mm)	m (mm)	Δr_{90} (mm)	Δm (mm)	ΔD_{max} (%)
250	250	40	0.04	0.09	2.2
250	250	100	0.40	0.75	1.6
250	250	160	0.42	5.44	2.0
250	207	100	0.90*	7.70*	–
225	206	40	1.00	1.10	3.0
225	206	100	0.50	1.50	2.0
225	206	140	0.80	3.00	1.7
225	166	100	1.50*	7.80*	–
200	165	160	2.17	0.01	1.5
200	165	100	2.15	2.46	1.9
200	165	140	2.27	1.97	1.8
200	138	60	1.60*	2.24*	–
180	137	40	2.05	1.89	2.3
180	137	60	2.12	0.59	2.0
180	137	100	2.22	1.35	2.5
180	111	60	1.13*	6.67*	–
160	110	20	2.05	0.17	3.0
160	110	40	2.03	2.76	2.8
160	110	60	2.02	3.47	3.0
160	110	80	2.07	2.13	2.2
160	110	100	2.11	0.23	1.0
160	85	60	1.06	3.47	3.0
140	84	40	0.61	0.78	1.9
140	74	60	0.69	1.30	2.9
120	63	40	1.07	1.85	1.9
120	63	20	1.24	0.12	2.6

E_p (MeV)	r_{90} (mm)	m (mm)	Δr_{90} (mm)	Δm (mm)	ΔD_{max} (%)
100	43	30	1.17	0.04	2.3
100	35	20	1.28	1.02	2.5

$\Delta r90$ is the absolute difference between the simulated and the measured ranges at the distal 90% dose location, Δm is the absolute difference in SOBP width ($\Delta r90$ and Δm values with an '*' were compared to the nominal values), and ΔD_{max} is the maximum absolute dose difference relative to the dose at the center of the SOBP.

Phys Med Biol. Author manuscript; available in PMC 2014 August 13.

Table 3

Comparison of simulated and measured lateral profiles for the large snout. E_p is the proton energy in MeV at nozzle entrance, m is the SOBP width of the SOBP in millimeters, and z is the depth of the profile relative to the upstream surface of the water phantom (isocenter) in millimeters. The absolute differences in the penumbra widths, denoted as $\Delta P_{90–10}$ for the values of the 90%–10% penumbras, $\Delta P_{90–50}$ for the values of the 90%–50% and $\Delta P_{80–20}$ for the absolute differences in the 80%–20% penumbras, are given in millimeters. The differences in field size, ΔFS, measured from the 50% to the 50% dose location, are also given in millimeters. The maximum dose difference, ΔD_{max}, in the high-dose region of the profile is given in percent of the dose normalized to the center of the profile.

E_p (MeV)	m (mm)	z (mm)	$\Delta P_{90–10}$ (mm)	$\Delta P_{90–50}$ (mm)	$\Delta P_{80–20}$ (mm)	ΔFS (mm)	ΔD_{max} (%)
250	40	248	1.14	0.53	0.96	0.52	0.9
250	40	228	1.41	0.63	1	0.58	0.8
250	40	208	1.37	0.69	0.79	0.51	0.9
250	100	248	1.34	0.61	1.04	0.3	1.0
250	100	199	1.32	0.68	0.89	0.53	0.9
250	100	149	0.68	0.17	0.35	0.52	0.9
250	160	248	1.17	0.63	1.02	0.54	1.0
250	160	163	0.93	0.55	0.38	0.5	1.0
250	160	83	0.33	0.28	0.37	0.13	0.9
250	100	206	1.64	1.07	0.93	0.24	1.5
250	100	157	0.92	0.45	0.52	0.36	1.0
250	100	107	0.15	0.01	0	0.47	0.8
225	40	166	1.33	0.54	0.66	0.57	1.0
225	40	186	0.97	0.64	0.85	0.58	0.9
225	40	205	1.77	0.89	0.91	0.85	1.5
225	100	108	0.39	0.03	0.03	0.49	1.0
225	100	157	1.21	0.52	0.63	0.69	1.0
225	100	205	1.89	0.99	0.92	0.73	0.8
225	140	65	0.32	0.23	0.35	0.33	0.9
225	140	135	0.85	0.3	0.44	0.59	0.9
225	140	205	2.01	1.13	0.97	0.79	1.0
225	100	65	0.30	0.27	0.27	0.24	0.9

E_p (MeV)	m (mm)	z (mm)	ΔP_{90-10} (mm)	ΔP_{90-50} (mm)	ΔP_{80-20} (mm)	ΔFS (mm)	ΔD_{max} (%)
225	100	116	0.66	0.10	0.25	0.49	1.0
225	100	165	1.29	0.56	0.61	0.61	1.0
200	40	124	0.45	0.28	0.53	0.59	1.9
200	40	144	1.78	1.02	1.11	1.55	1.5
200	40	164	1.55	1.14	0.69	0.52	1.8
200	100	115	1.14	0.50	0.61	0.57	1.3
200	100	164	1.89	1.15	0.78	0.41	1.8
200	140	60	0.59	0.02	0.17	0.57	1.1
200	140	94	0.46	0.32	0.18	0.52	0.7
200	60	78	0.15	0.16	0.07	0.22	2.2
200	60	108	0.85	0.48	0.40	0.17	0.9
200	60	137	1.21	0.77	0.68	0.04	3.5
180	40	98	0.22	0.05	0.09	0.56	2.5
180	40	117	0.88	0.33	0.44	0.65	2.0
180	40	135	1.36	0.73	0.72	0.69	3.0
180	60	78	0.30	0.11	0.08	0.28	1.5
180	60	107	0.79	0.32	0.40	0.66	2.4
180	60	135	0.77	0.47	0.56	0.18	2.6
180	100	60	0.39	0.19	0.24	0.36	1.3
180	100	85	0.32	0.13	0.12	0.56	1.0
180	100	135	1.43	0.82	0.83	0.73	3.0
180	60	60	0.10	0.18	0.17	0.44	1.0
180	60	80	0.02	0.06	0.02	0.29	0.9
180	60	110	0.96	0.54	0.60	0.76	4.0
160	40	70	0.04	0.20	0.07	0.53	2.3
160	40	90	0.03	0.08	0.01	0.17	2.6
160	40	108	0.14	0.20	0.01	0.08	3.0
160	80	68	0.39	0.26	0.32	0.25	2.1
160	80	108	0.04	0.19	0.16	0.04	3.0
160	60	60	0.34	0.14	0.19	0.36	2.4
160	60	80	0.06	0.00	0.03	0.49	2.7

E_p (MeV)	m (mm)	z (mm)	ΔP_{90-10} (mm)	ΔP_{90-50} (mm)	ΔP_{80-20} (mm)	ΔFS (mm)	ΔD_{max} (%)
140	40	64	0.17	0.13	0.16	0.31	2.1
120	40	43	0.21	0.12	0.03	0.43	2.0
100	30	12	0.49	0.34	0.32	0.05	3.0
100	30	28	0.11	0.15	0.01	0.54	1.5

Table 4

Comparison of simulated and measured PDDs and lateral profiles for the inhomogeneous geometry. E_p is the proton energy in MeV at nozzle entrance. SOBP width m of the SOBP was 10 cm in all cases;, and z is the depth of the profile relative to the upstream surface of the water phantom (isocenter) in millimeters. Δr is the absolute difference in range at the distal 90% dose location. The absolute differences in penumbra widths are denoted as $\Delta P_{80–20}$ for the 80%–20% penumbras. The maximum dose difference, ΔD_{max}, in the high-dose region of the profiles is given as a percentage of the dose normalized to the center of the profile. In the case of PDDs, the maximum dose difference was given as a percentage of dose normalized to the values at the center of the SOBP.

Type	E_p (MeV)	Δr (mm)	z (mm)	$\Delta P_{80–20}$ (mm)	ΔD_{max} (%)
PDD	225	0.67	–	–	2.0
PDD	200	1.50	–	–	1.0
PDD	180	0.94	–	–	1.0
PDD	180*	1.28	–	–	1.3
LatProf	225	–	208	1.36	1.5
LatProf	200	–	162	0.43	1.5
LatProf	180	–	133	0.25	1.5
LatProf	180*	–	108	0.15	1.6

The E_p values with asterisks were measured and simulated with the full set of range shifter plates in the beam to deliver a beam with minimum range (for 180 MeV) in the phantom.